ISIMA 2010

The Orbital Decay of a Retrograde Planet Embedded in a Protoplanetary Disk

Jeffrey Fung (University of Toronto)
Supervised by Clément Baruteau (University of California Santa Cruz)

Abstract

Motivated by recent observations of retrograde planets, we investigated the orbital decay of a retrograde planet embedded in a protoplanetary disk. We treated both gravitational and hydrodynamic drag, and found the migration time scale ranges from 10^3 to 10^5 years for planet masses between 10^{-3} to 10^1 Jupiter masses. We also found that a highly inclined orbit can increase this time scale by a factor of 10, and that due to inclination damping, the final inclination is unlikely to be greater than $50°$.

1 Background

In recent years, observations of transiting hot Jupiters and determinations of their orbital properties has led to discoveries of planets whose orbits are likely in retrograde motion with respect to the rotation of their host stars [1][2][3][4][5]. The direction of a transiting planet's rotation axis can be constrained through a measurement of the Rossiter-McLaughin effect, which describes the overall red-shift of the star's spectrum while the planet is blocking star light from the blue-shifted side, and vise-versa. In Triaud et al 2010 [1], among the 6 planets examined, 3 of them showed a high probability of having retrograde orbits. This is in contradiction to the naive expectation that all planets should be prograde since the original accretion disk must be prograde.

Possible methods for creating retrograde planets include the Kozai mechanism and planet-planet scattering. The Kozai mechanism describes the precision of a circumbinary planet's orbit, which can in time increase its inclination to over $90°$. Planet-planet scattering, on the other hand, can alter the orbit properties of a planet abruptly and potentially create retrograde orbits in a time-scale of order 10^4 years or less [6]. In this project we study the interaction between a retrograde planet and a protoplanetary disk, which has a lifetime of order 10^7 years. The Kozai mechanism does not apply here since we consider a single-star system, also the Kozai mechanism requires a highly inclined orbit initially, moreover, it is a slow process which cannot convert a planet into retrograde motion within the lifetime of the protoplanetary disk. Planet-planet scattering, on the other hand, can likely be the cause of a system like the one we study; however, we will assume there is only one planet in the system for simplicity. One can assume the gravitational interaction between a prograde and a retrograde planet to be a small effect since the time they can spend in proximity is a small fraction to their orbital periods.

2 The Drag Forces

As the planet travels in the gas disk, it interacts with the disk in two ways: hydrodynamical interaction and gravitational interaction. Both of them can be described as drag forces acting on the planet. For an object traveling in a fluid, the drag force it experiences can generally be written in the following way:

$$F_{\mathrm{D}} = I\rho\sigma u^2, \tag{1}$$

where I is the drag coefficient, ρ is the unperturbed density of the fluid, σ is the cross section of the object, and u is the relative velocity between the object and the fluid.

I is in general dependant on the geometric shape of the object, the properties of the fluid, and u. The relative velocity between a retrograde planet and a prograde gas disk is two times the Keplerian velocity, v_{k}. It is safe to assume the gas disk moves at Keplerian velocity since the change in velocity due to pressure support is only a few percent. One can express the relative velocity as a Mach number. The sound speed, c_{g}, in the disk can be estimated as:

$$c_{\mathrm{g}} = \frac{H}{r} v_{\mathrm{k}}, \tag{2}$$

where H is the pressure scale height and r is distance from the location in space to the central star projected on the midplane. One can assume $H \sim 0.05r$, resulting in $c_{\mathrm{g}} = 0.05 v_{\mathrm{k}}$, which gives a Mach number of 40. Note that this number remains a constant as long as the eccentricity of the orbit remains zero.

In the following sections we will describe the two kinds of drag force, keeping in mind the planet's motion is highly supersonic.

2.1 Hydrodynamic Drag

The hydrodynamic drag is caused by the gas pressure exerted on the planet through physical contact, much like the aerodynamic drag a plane would experience when flying. Adachi et al 1976 [7] solved the problem of the orbital decay of a planetesimal traveling in a protoplanetary disk, and the very same physics applies here as well. Revisiting Eq.(1), the cross section of the planet is simply its surface area projected on 2D, $\sigma = \pi r_{\mathrm{p}}^2$, where r_{p} is the radius of the planet. The drag coefficient I for a sphere at a supersonic speed is a constant equals to one [7]. Therefore the hydrodynamic drag can be written as:

$$F_{\mathrm{Hydro}} = 4\pi\rho r_{\mathrm{p}}^2 v_{\mathrm{k}}^2 \tag{3}$$

However, if the planet in question is a gas giant, then it is not true that it is a solid object with a spherical shape. In fact, the planet should be accreting gas, therefore it is unclear how should one define its shape or mass. For simplicity, we will assume $I = 1$ holds, meaning the planet is a solid spherical object, and its mass remains constant. The effects of hydrodynamic drag on a gaseous body will be the object of a future investigation.

2.2 Gravitational Drag (Dynamical Friction)

Gravitational drag is the same as the dynamical friction studied by Chandrasekhar, and is described by the well-known Chandrasekhar's formula for dynamical friction [11]. This formula essentially describes the deceleration of a perturber traveling in a homogenous and isotropic collisionless medium due to gravitational interaction using linear perturbation theory. Ostriker 1999 [8] extended the theory for a collisional medium; Kim & Kim 2007 [9], then confirmed Ostriker 1999's formulism also applies in the case when the object is moving in a circular orbit.

In terms of Eq.(1), the cross section can be written as the surface area of a shell with radius equal to the Bondi radius of the object, $r_{\rm B} = \frac{GM_{\rm p}}{u^2}$, so $\sigma = 4\pi r_{\rm B}^2$.

The drag coefficient I is equal to the Coulomb logarithm, $\ln(\frac{r_{\rm max}}{r_{\rm B}})$, in Chandrasekhar's formula. Ostriker 1999 showed that for a highly supersonic perturber this relation holds in a collisional fluid. Kim & Kim 2009 [10] did a numerical study of this problem, and empirically determined a correction factor which can be included in I:

$$I = \left(\frac{2r_{\rm s}}{r_{\rm B}}\right)^{0.45} \ln\left(\frac{r_{\rm max}}{r_{\rm B}}\right), \tag{4}$$

where $r_{\rm s}$ is the softening length used in the simulation, and $r_{\rm max}$ is the length scale of the perturbed medium. The choice of $r_{\rm max}$ is somewhat arbitrary, but for a circular orbit it is common to take it as equivalent to the semi-major axis, a. Note that the correction factor depends on the softening length, indicating it could be a numerical artifact. In general $r_{\rm s}$ is a not a very small fraction of $r_{\rm B}$, as a result $\left(\frac{2r_{\rm s}}{r_{\rm B}}\right)^{0.45} \sim 1$. Since the softening length is not a physical quantity and the correction term is close to unity, it is reasonable to leave it out. An expression for the drag force is then given as:

$$F_{\rm Grav} = \ln\left(\frac{a}{r_{\rm B}}\right) 16\pi\rho r_{\rm B}^2 v_{\rm k}^2 \tag{5}$$

2.3 Comparing the Two Drag Forces

If one divide Eq.(6) by Eq.(3), one gets:

$$\frac{F_{\rm Grav}}{F_{\rm Hydro}} = 4\ln\left(\frac{a}{r_{\rm B}}\right)\left(\frac{r_{\rm B}}{r_{\rm p}}\right)^2. \tag{6}$$

For a Jupiter-sized planet at 10AU, $\ln\left(\frac{a}{r_{\rm B}}\right) \sim 7$, and $\frac{r_{\rm B}}{r_{\rm p}} \sim 2$. Therefore the gravitational drag is about 100 times stronger than the hydrodynamic drag.

When $r_{\rm B} > r_{\rm p}$, there is an additional reason why the hydrodynamic drag is unimportant. The object generates a detached bow shock traveling ahead of itself at a distance $\sim r_{\rm B}$. As long as $r_{\rm B} > r_{\rm p}$, the gas entering the shock will be in subsonic motion with respect to the planet, rendering the hydrodynamic drag very weak. On the other hand, if $r_{\rm B} < r_{\rm p}$, then the bow shock is pressed onto the surface of the planet, and hydrodynamic drag cannot be neglected any longer. The total drag force can therefore be expressed as:

$$F_{\rm D} = \begin{cases} F_{\rm Grav}, & r_{\rm B} > r_{\rm p} \\ F_{\rm Grav} + F_{\rm Hydro}, & r_{\rm B} \leq r_{\rm p} \end{cases}. \tag{7}$$

Another important point is that the Bondi radius decreases with increasing relative velocity. As the planet migrates inward, the relative velocity increases since the Keplerian velocity increases, and the Bondi radius shrinks. This means the hydrodynamic drag eventually becomes the dominant force regardless of the beginning position of the planet.

3 Evolution of a, e, and i

Given the drag force, it is possible to determine how the semi-major axis a, eccentricity e, and inclination i evolve in time. Here we define i as the angle between the plane of the gas disk and the orbital plane of the retrograde planet; i.e. $i = 0$ means the planet is in retrograde motion but orbits in the midplane of the gas disk.

We start by writing the drag force in vector notation:

$$\vec{F_{\rm D}} = -I\rho\sigma|\vec{u}|\vec{u}, \tag{8}$$

Given a, e, and i, $\vec{u}$ can be determined. In cylindrical coordinate:

$$u_{\rm R} = \sqrt{\frac{GM_*}{a(1-e^2)}} e \sin\psi, \tag{9}$$

$$u_{\psi} = \sqrt{\frac{GM_*}{a(1-e^2)}} (1 + e\cos\psi) + \sqrt{\frac{GM_*}{r}} \cos i, \tag{10}$$

$$u_{\rm z} = \sqrt{\frac{GM_*}{r}} \sin(i) \cos(\psi + \psi_o), \tag{11}$$

where R, ψ and z are the cylindrical coordinates where $z = 0$ is the orbital plane of the planet; ψ_o is a constant describing the phase difference between e and i; and M_* is the mass of the host star.

The density distribution of the gas disk can be modeled by a flaring thin disk in hydrostatic equilibrium:

$$\rho = \rho_o \left(\frac{r}{1AU}\right)^{-\frac{3}{2}} e^{-\left(10\frac{z}{r}\right)^2}, \tag{12}$$

where $\rho_o \sim 10^{-9} g\ cm^{-3}$ and:

$$z = \frac{a(1-e^2)}{1+e\cos\psi}\sin(i)\sin(\psi+\psi_o) \tag{13}$$

$$r = \frac{a(1-e^2)}{1+e\cos\psi}\sqrt{1-\sin^2(i)\sin^2(\psi+\psi_o)} \tag{14}$$

The equations for the evolution of a, e, and i can be written as [12]:

$$\frac{\mathrm{d}a}{\mathrm{d}\psi} = \frac{2a}{GM_*(1-e^2)}\left(\frac{a(1-e^2)}{1+e\cos\psi}\right)^2 \left(F_{\mathrm{R}} e\sin\psi + F_\psi(1+e\cos\psi)\right), \tag{15}$$

$$\frac{\mathrm{d}e}{\mathrm{d}\psi} = \frac{1}{GM_*}\left(\frac{a(1-e^2)}{1+e\cos\psi}\right)^2 \left(F_{\mathrm{R}}\sin\psi + F_\psi\left(\frac{1-e^2}{e} - \frac{1-e^2}{e+e^2\cos\psi}\right)\right), \tag{16}$$

$$\frac{\mathrm{d}i}{\mathrm{d}\psi} = \frac{1}{GM_*(1-e^2)}\left(\frac{a(1-e^2)}{1+e\cos\psi}\right)^2 F_{\mathrm{z}}\frac{1-e^2}{1+e\cos\psi}\cos(\psi+\psi_o). \tag{17}$$

Since we have an exact description of the drag force, these equations can be integrated to give an exact solution to the problem.

3.1 Limitations of the Model

In this model we assumed the gas disk always remain in the unperturbed state. This assumption is only valid if the disk can recover from the perturbation within the time of one orbital period. While the Bondi radius is small compared to the semi-major axis, implying the perturbation is strong only in a small scale, it is unclear how quickly does the disk recover. Therefore our assumption here does require further examination.

Another limitation to this model is the drag force description is not valid in an accelerating frame, which would be the case if e is non-zero. Fundamentally the reason for this invalidity is that when the orbit of the planet is eccentric, the angular momentum of the gas is no longer conserved, and therefore Chandrasekhar's formula is no longer valid.

To overcome these limitations it requires one to numerically simulate, solve and analyze the problem. Nonetheless, solving Eq.(15) and Eq.(17) can give us insight into the orbital decay of circular retrograde orbits.

3.2 Results

We solved Eq.(15) and Eq.(17) with different planet masses, different initial semi-major axes and inclinations. Fig.1(a) shows the migration time for a planet initially located at 10AU to reach 0.1AU as a function of planet mass. When the planet mass is 0.001 Jupiter mass, migration time increases as planet mass increases. This is because when the planet mass is small, it is in the hydrodynamic drag dominant regime. Given the average density of the planet is a constant, $F_{\mathrm{D}} \propto r_{\mathrm{p}}^2 \propto M_{\mathrm{p}}^{\frac{2}{3}}$, which means the deceleration rate is proportional to $M_{\mathrm{p}}^{-\frac{1}{3}}$, meaning migration is slower with increasing mass.

For planet mass above 0.005 Jupiter mass, gravitational drag is the dominant drag force. Since the Bondi radius is directly proportional to the planet mass, the deceleration rate is also directly proportional to the planet mass, resulting in the shortening of the migration time as mass increases.

Note that in Fig.1(a) the migration times are very short, not even exceeding 10^5 years. It is however, possible to increase this timescale by introducing an inclination to the orbit.

Fig.1(b) describes the increase of the migration time scale we introduce a larger and larger initial inclination to the orbit. Calculation was done for a planet of one Jupiter mass initially with a semi-major axis of 10AU. One sees that if the initial inclination is as large as 80°, the migration time is nearly 10 times longer than with zero inclination. The final inclinations for the same initial conditions are plotted on Fig.1(c). It is worth noting that even with an initial inclination as large as 80°, the final inclination does not exceed 25°.

Next we looked at how the final inclination varies with initial semi-major axis. The result is plotted on Fig.1(d). The planet in each case has one Jupiter mass and an initial inclination of 80°. Naturally the shorter the initial semi-major axis is the shorter the migration time becomes, and the less time is available for inclination damping. However, even if the planet is initially placed at 1AU, the final inclination is still significantly damped from 80° to 45°.

The retrograde planets observed all tend to have large inclination. In particular, the 3 retrograde planets discovered by Triaud et al 2010 [1] all have an inclination larger than 50°, which is unlikely to happen in our model. This could imply inclination pumping that occurs after the gas disk had evaporated.

4 Local Simulations

As suggested before, a global simulation needs to be done to obtain a thorough understanding of the problem. However, there are technical difficulties that must first be overcome. Mainly, the resolution needed for even a 2-dimensional simulation of this problem is overwhelmingly high. Since the main scale of this problem is the Bondi radius, we need to resolve this length; however, the Bondi radius is typically a hundred times shorter than the semi-major axis of the orbit. If we put 10 grid cells in one Bondi radius, the entire grid would have the ridiculous size of 10^4 by 10^4. Before this difficulty is resolved, it is useful to first do some local simulations of the problem.

Since the simulation will be in 2D, it should be noted that the drag force is different in 2D than in 3D. Namely, the cross-section is different. Here is a comparison of the 3D and 2D drag forces:

$$F_{Grav}^{3D} = I^{3D}\rho(4\pi r_B^2)u^2, \tag{18}$$

$$F_{Grav}^{2D} = I^{2D}\Sigma(2\pi r_B)u^2, \tag{19}$$

where Σ is the surface density of the disk. Note that in 2-dimension, the gravitational drag force depends only on one factor of r_B, which means it is linearly dependent of the planet mass. I^{2D} is unknown, but can be determined empirically through simulations.

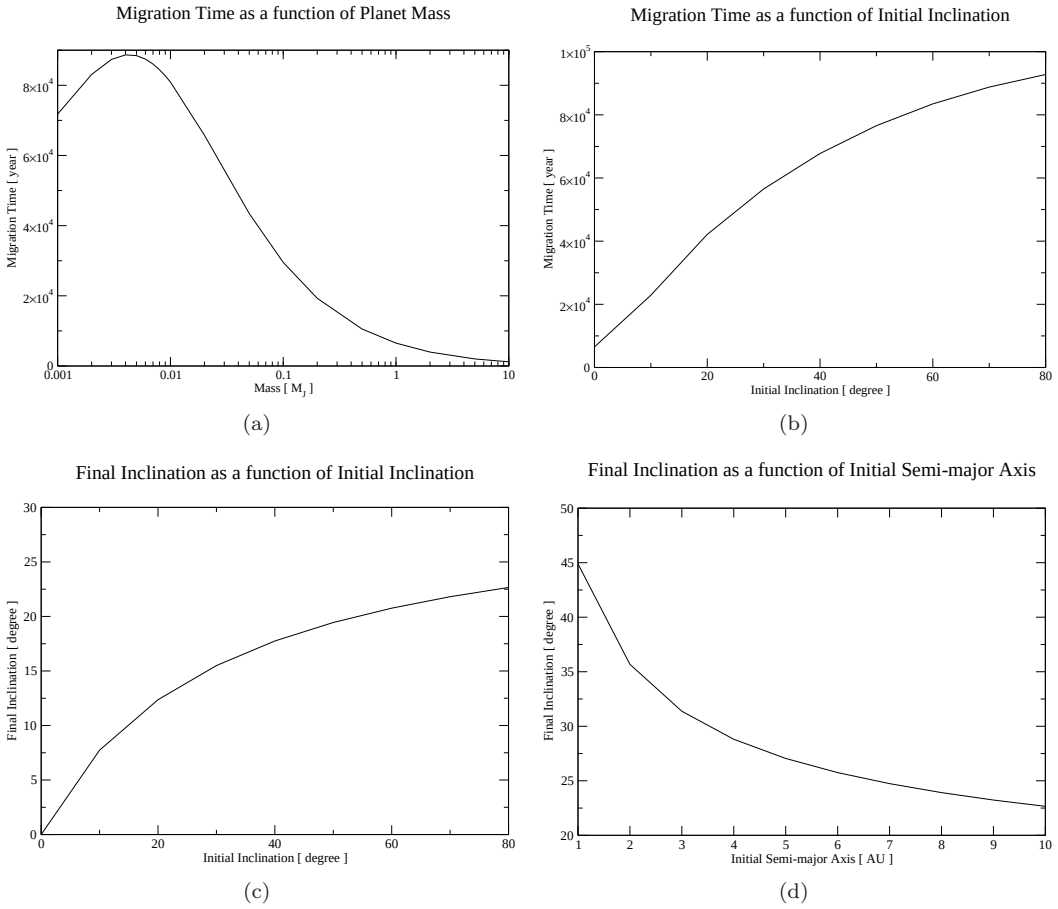
Migration Time as a function of Planet Mass
Migration Time [year]
Mass [M_J]
(a)
Migration Time as a function of Initial Inclination
Migration Time [year]
Initial Inclination [degree]
(b)
Final Inclination as a function of Initial Inclination
Final Inclination [degree]
Initial Inclination [degree]
(c)
Final Inclination as a function of Initial Semi-major Axis
Final Inclination [degree]
Initial Semi-major Axis [AU]
(d)

Figure 1:

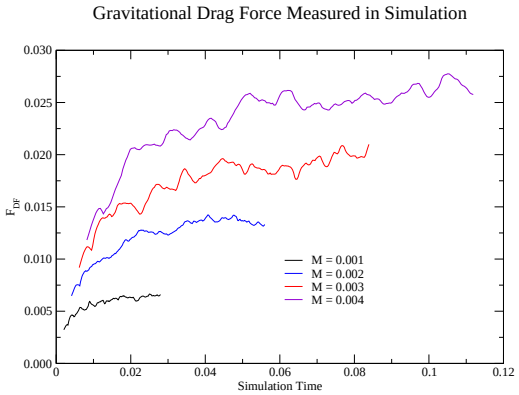

Figure 2:

4.1 Results

The simulations were done on a 488x732 grid, solved with the piece-wise parabolic method. Fig.2 is a plot of the measured drag force in for different runs, each with a different planet mass. One sees that the result matches Eq.(19) in that the force scales linearly with planet mass. A preliminary measurement of I^{2D} gives $I^{2D} \approx 1$, but more runs should be done to confirm this.

5 Conclusion

An analysis of the planet-disk interaction in the case of a retrograde planet is done. We find the migration time of such a planet to be much shorter than the lifetime of a typical protoplanetary disk. Therefore we expect a low likelihood of finding retrograde planets at radii larger than the hot Jupiter range. We also find the inclination of a retrograde orbit is damped significantly during migration, and that even with extreme initial inclination the final inclination is unlikely to be over 50°. Since this is inconsistent with observation, it is possible that the inclination can be pumped later through other mechanisms such as planet-planet interaction.

The next stage for this project will be to do a global simulation of the migration of a retrograde planet. The difficulty with resolution could be solve through a rescaling of the problem by assuming a high-mass planet. Another related problem is to examine in detail the atmosphere of a retrograde planet. The drag forces exerted on the planet should heat up its atmosphere and potentially even strip it away. On the other hand, gas accretion is also at work. The dynamics in this problem also apply to prograde gas giants in eccentric orbits.

References

[1] Triaud, Amaury H. M. J.; Collier Cameron, A.; Queloz, D.; Anderson, David R.; Gillon, M.; Hebb, L.; Hellier, C.; Loeillet, B.; Maxted, Pierre F.; Mayor, M.; Pepe, F.; Pollacco,

D.; Sgransan, D.; Smalley, B.; Udry, S.; West, Richard G.; Wheatley, Peter J., 2010, eprint arXiv:1008.2353

[2] Anderson, D. R.; Hellier, C.; Gillon, M.; Triaud, A. H. M. J.; Smalley, B.; Hebb, L.; Collier Cameron, A.; Maxted, P. F. L.; Queloz, D.; West, R. G.; Bentley, S. J.; Enoch, B.; Horne, K.; Lister, T. A.; Mayor, M.; Parley, N. R.; Pepe, F.; Pollacco, D.; Sgransan, D.; Udry, S.; Wilson, D. M., 2010, The Astrophysical Journal, 709, 1, 159-167

[3] Narita, N.; Sato, B.; Hirano, T., Tamura, M., 2009, Publications of the Astronomical Society of Japan, 61, 5, L35-L40

[4] Winn, Joshua N.; Johnson, John A.; Albrecht, S.; Howard, Andrew W.; Marcy, Geoffrey W.; Crossfield, Ian J.; Holman, Matthew J., 2009, The Astrophysical Journal Letters, 703, 2, L99-L103

[5] Queloz, D.; Anderson, D.; Collier Cameron, A.; Gillon, M.; Hebb, L.; Hellier, C.; Maxted, P.; Pepe, F.; Pollacco, D.; Sgransan, D.; Smalley, B.; Triaud, A. H. M. J.; Udry, S.; West, R., 2010, Astronomy and Astrophysics, 517, id.L1

[6] Wu, Y.; Murray, N., 2003, The Astrophysical Journal, 589, 1, 605-614

[7] Adachi, I.; Hayashi, C.; Nakazawa, K., 1976, Progress of Theoretical Physics, 56, 6

[8] Ostriker, Eve C., 1999, The Astrophysical Journal, 513, 252-258

[9] Kim, H.; Kim, W., 2007, The Astrophysical Journal, 665, 1, 432-444

[10] Kim, H.; Kim, W., 2009, The Astrophysical Journal, 703, 2, 1278-1293

[11] Binney, J.; Tremaine, S., *Galactic Dynamics*, Second Edition, 2008, Princeton University Press, Princeton, ISBN-13: 978-0-691-13027-9

[12] Brouwer, D.; Clemence, G. M., *Method of Celestial Mechanics*, 1961, Academic Press, New York